

Tracking physiological changes in an in-vivo model of Epilepsy: A Model-Based Approach

R.S. Balson

September 3, 2013

1 Introduction

Aims

Estimate model parameters from a neural mass model of the hippocampus. At present, the mechanisms underlying the generation of epileptic seizures are unknown, and approximately one third of patients with epilepsy are refractory to treatment. In this paper, a new method to estimate physiological properties of the brain is introduced. This method involves the application of a well established neural mass model with a new estimation technique. In particular, the application of an unscented Kalman filter (UKF) (Voss et al., 2004) for estimation of physiologically relevant parameters from a neural mass model of the hippocampus (Wendling et al., 2002) (referred to as the “Wendling model”) using EEG recordings is considered. It is hypothesised that, using the UKF, parameters from the Wendling model can be tracked with simulated noisy observations.

To improve the understanding of epilepsy and improve the treatment of epilepsy patients. Estimating physiologically descriptive parameters from the Wendling model will make it possible to approximate changes occurring in the brain that lead to seizures. This will be achieved by estimating model parameters based on electrographic recordings of seizures from the hippocampus. Further, this method can be applied to determine the effect that treatment has on the brain, by observing changes in the estimated model parameters. Approximating the brain’s physiology in this manner will make it possible to titrate therapies that are patient-specific and optimise their efficacy. For example, if, in a specific patient, it is found that a specific parameter space is estimated for most seizures, then a treatment strategy that forces the model parameters away from this space can be determined.

How has this been achieved previously?

Introduction to neural mass model, freeman, jansen etc Neural mass models, originally formulated in the early 1970’s (Wilson and Cowan, 1973; Lopes da Silva et al., 1974; Freeman, 1963) and developed subsequently (Jansen and Rit, 1995), describe a cortical region of the brain as having populations of inhibitory and excitatory neurons. The net dynamics of the soma and synapses of neural populations are modeled by two functions. The first function describes how a synapse reacts to an firing rate in terms of a propagation delay and a synaptic gain, and takes the form of an integral kernel. The delay specifies the time taken for action potentials to propagate from one population to the next through dendritic trees, and the synaptic gain is a measure of the membrane potential magnitude resulting from a single action potential arriving at the considered population. The second function describes how the membrane potential of each neural population is converted into a firing rate. The firing rate specifies the average number of action potentials generated from

the considered population. The second function is modeled as a sigmoid, which was originally formulated to describe the probability of a neuron firing given a specific membrane potential. In this case, population dynamics are considered; therefore, the sigmoid output is a firing rate, which is dependant on a population's membrane potential. Lastly, the number of synaptic connections linking neural populations together is specified by a connectivity constant.

What is the output of the model and why Neural mass models are phenomenological models of EEG, that describe the dynamics of excitatory and inhibitory populations. Excitatory neurons primarily consist of pyramidal neurons [ref](#)which are known to have similar orientations. The parallel orientation of the pyramidal neurons allows for the electrical fields that they produce to sum together. For other neural populations, orientation is random and their net effect on the measured electric field is minimal. Therefore, the excitatory neural population is the generator of observed EEG.

Is a neural mass model a good model Are neural mass models, good models of the brain? To answer this question a definition for the word model is required. In this paper a model is considered to be an approximate descriptor of a system, which in this case is the brain. Since neural mass models are derived from aspects of neural physiology they can be considered to be models of the brain. Whether they are good models of the brain depends on how well they are able to replicate the observations they are intended to mimic. That being said a good neural mass model is merely one of numerous descriptors of the brain, and without further evaluation of the results obtained from the model with physiological studies a model provides little evidence of causal relationships. However, by using these models insight can be gained into what aspects of physiology should be evaluated, and can provide a method for aspects of physiology that can not normally be observed, to be crudely estimated. For this study, a good model will be considered to be any model that can describe normal and seizure EEG with distinctly different physiological properties. Further, this model should account for all relevant physiological studies that have demonstrated causal physiological effects that would affect the considered model of the brain.

Inadequacy of jansen model and intro to the wendling model Neural mass models have been shown to be capable of reproducing key phenomena observed in EEG. A model proposed by Jansen and Rit (1995) was shown to be capable of replicating normal EEG as well as alpha waves by altering a subset of its model parameters. Further studies have shown that by altering different parameters the model could replicate almost all activity observed in EEG. When considering the hippocampus, a study performed by White et al. (2000) showed that within the hippocampus the effect of inhibition on the pyramidal population had two distinctly different propagation delays, and that both were significant for the reproduction of EEG. They hypothesised that the cause of the

two different propagation delays were due to the location of the synapses connecting the inhibitory and pyramidal populations. Longer propagation delays are due to synapse connections far from the soma (peri-dendritic), and shorter delays are due to connections near the soma (peri-somatic). The different propagation delays of inhibitory populations in the hippocampus was incorporated into the neural mass model by Wendling et al. (2002). To account for the two propagation delays Wendling et al. (2002) described two different types of inhibitory populations: one fast (peri-somatic), and the other slow (peri-dendritic). In the same study, it was shown that the addition of the peri-somatic inhibitory population made it possible to replicate almost all types of observed EEG by altering three model parameters.

This model is capable of replicating key characteristics observed in EEG prior to and during seizure.

The Wendling model is capable of replicating key features observed in EEG prior to, during, and after seizures. This is achieved by altering physiological parameters that describe the balance between excitation and inhibition in the modeled region of the brain. Due to its description of neuronal connections and systems in terms of neural populations, the model only has ten parameters, of which three describe the balance between excitation and inhibition (Wendling et al., 2002). By altering the three parameters describing the balance between inhibition and excitation almost all phenomena in EEG can be mimicked. Therefore, to imitate the observed output of iEEG, it is necessary to be able to estimate these three model parameters.

Is the Wendling model a good model

The Wendling model is considered to be a good model of the hippocampus since it is capable of mimicking the key features required for this study, and has a strong link to the physiology in the hippocampus. One further advantage of this model is that only three parameters need to be altered to imitate EEG, which will allow for more accurate estimation. The reason for this is that as the number of parameters estimated increases so does the complexity and inaccuracy of estimation. This is particularly important when considered estimation of real data, where the model is merely an approximation of the observations. If the number of parameters is large for this estimation there is bound to be large errors, due to numerous local minima in the cost function.

Previous work on estimating the neural mass model of the hippocampus has been done using a genetic algorithm.

Estimation of the neural mass model (Genetic Algorithm)

Estimating the model parameters in the Wendling model is non-trivial. This is due to the nonlinear structure of the sigmoid function, as well as the stochastic input in the model. The neural mass model of the hippocampus has previously been estimated using the genetic algo-

rithm (Wendling et al., 2005), which is capable of estimating model parameters iteratively. The iterative procedure ensures that the genetic algorithm converges, although it may converge to the incorrect parameters. For the the genetic algorithm to converge, the data analysed needs to be stationary, i.e. model parameters need to be constant over the considered period of observations.

Kalman filter Another estimation method known as Kalman filtering allows the estimation of parameters in real time. The Kalman filter updates model parameters based on each observation made, and approximate the most likely model parameters that could have resulted in the current observation. However, the Kalman filter can only be applied to linear system estimation. This led to the development of new estimation techniques derived of the Kalman filter. One method is the UKF which approximates the system nonlinearity [ref](#). This approximation has been shown to be accurate in many studies [ref](#).

Why the Kalman filter The advantage of the UKF over the genetic algorithm is that there is no requirement that the observations are stationary, as it can track the changes in model parameters. This is important as subtle changes in model parameters may give an indication of when a seizure is about to occur, and could provide evidence of the effect of therapeutic treatments on the brain's physiology. These features of the UKF may allow for it to be implemeted in applications such as seizure prediction and responsive stimulation This is not possible using the genetic algorithm as it is an iterative estimation technique.

What is being done, and why is it better or different?

In this paper, the application of the UKF for the estimation of the three model parameters describing the balance between excitation and inhibition is considered. Initially, EEG is simulated using the Wendling model, which is then used as the observations for the estimation procedure. Model parameters are then estimated, under the assumption that they were originally unknown. The robustness of the estimation procedure is determined by evaluating the accuracy of estimation under conditions where observation noise is varied and states are initialised with of errors from their actual values.

What is being done with the UKF The UKF, unlike the genetic algorithm, does not rely on iteration and is less time consuming. This computational efficiency comes at the cost of accuracy. This paper looks at the accuracy of the filter under numerous conditions to determine how robust it is. If the UKF is accurate at tracking model parameters then this method could be used to help characterise full EEG data sets, and allow for treatments to be evaluated and developed. This method may allow for patient specific treatments to be developed.

Structure of the paper In the methods section, a description of the neural mass model of the hippocampus is presented, as well as the equations used to simulate the model. Further, the for-

mulation of the UKF for the Wendling model is described. In the results section, the performances of the algorithm under numerous conditions are demonstrated. Lastly, in the discussion section, an evaluation of the performance of the filter is provided, discussing whether this method is a viable way forward to use model estimation to help approximate the effect that disorders and treatments have on the brain.

Model estimation and accuracy for real data

2 Methods

What we are doing in this paper The Wendling model is capable of mimicking normal and seizure activity observed in hippocampal EEG in people with epilepsy (Wendling et al., 2002, 2005). Here, the estimation of physiologically relevant model parameters from the Wendling model is considered. An unscented Kalman filter (UKF) is used to estimate the model parameters of interest. For this study, the estimation procedure is tested using EEG simulated from the Wendling model to determine the robustness of the UKF.

2.1 Model Description and Simulation

Wendling model description. The Wendling model describes the aggregate membrane potentials and firing rates produced by different neural populations. Each neural population is either excited or inhibited by other populations in the model. The net effect of one population on another is determined by a scaling constant termed connectivity. A graphical representation of the model is shown in Figure 1. In the model, four different neural populations are considered. The pyramidal neural population is the generator of EEG. Excitatory interneurons excite the pyramidal neurons (this connection is often modelled as a time delayed recurrent connection of the pyramidal population). Slow and fast inhibitory interneurons suppress the pyramidal neural population. The pyramidal neural population excites the excitatory and slow and fast inhibitory populations. Slow inhibitory interneurons suppress the fast inhibitory neural population. The effect of each neural population on the other is scaled by connectivity that accounts for the number of afferent synaptic connections between neural populations. A stochastic input to the model is added to account for the unknown effect of afferent pyramidal neurons from other areas of the brain.

Mathematical functions used in the model The Wendling model consists of two functions. The first function is a sigmoid function, which converts an aggregate membrane potential to an average firing rate,

$$g(v(t)) = \frac{g_{max}}{1 + \exp(r(v(t) - v_0))}, \quad (1)$$

where g_{max} is the maximum the firing rate, r is the sigmoid gradient, and v_0 is the membrane potential at which $0.5g_{max}$ is attained. The sigmoid function describes the response of a neuron's soma to a given membrane potential. To understand this sigmoid shape, conceptually it can be seen as the integral of a normal distribution. When considering a neural population there are numerous neurons which can be described by different sigmoid functions. The resulting sigmoid shape is a

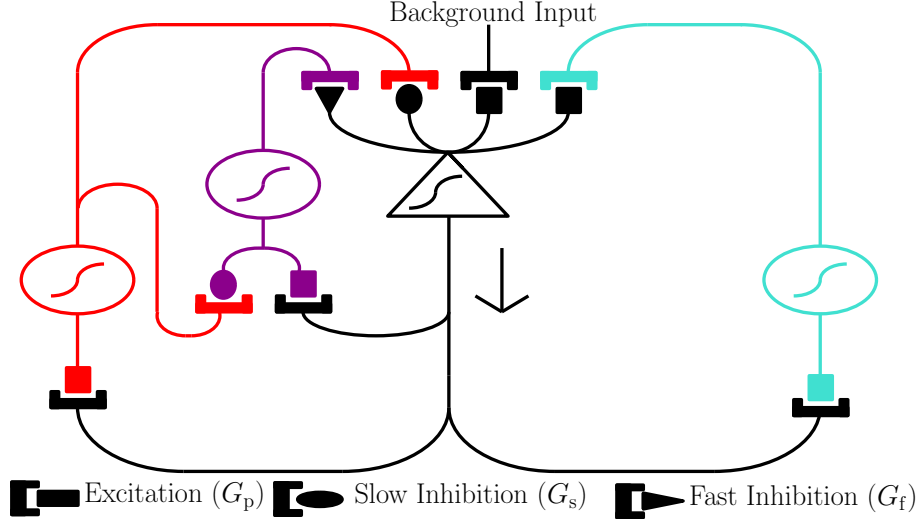


Figure 1: Graphical Description of the Wendling model. Membrane potentials are shown and named v_b where b is p, e, f and s for pyramidal, excitatory, and fast and slow inhibitory populations, respectively. The synaptic gains of each population are specified by G_m where m is defined in the same manner as the membrane potentials and $G_p = G_e$. The triangle shape indicates the pyramidal population and the circle shapes represent interneurons. Each line indicates a neural connection, which is specified by a connectivity constant.

summation of the expected number of neurons that will fire given a specific membrane potential. The second function is an average firing rate to population membrane potential integration kernel

$$v_b(t) = G_b(t)h_b(t) * g(v(t)) \quad (2)$$

$$h_b(t) = \begin{cases} \frac{1}{\tau_b} t \exp\left(-\frac{t}{\tau_b}\right) & t \geq 0 \\ 0 & t < 0 \end{cases}. \quad (3)$$

Here, $v_b(t)$ is the aggregate membrane potential, $h_b(t)$ is a kernel that converts firing rates to membrane potentials, $G_b(t)$ is the synaptic gain, and τ_b is the time constant. The operator $*$ represents a convolution. The function $h_b(t)$ is a time delayed exponential decay function (Figure 2). The subscript b is used to indicate that each neural population is described with a different synaptic gain and time constant. The synaptic gains are time dependant as they are the parameters that are altered to simulate different EEG characteristics (figure 4). In this description of the Wendling model, numerous model parameters are considered to be stationary: the maximum firing rate (g_{max}), threshold voltage (v_0), sigmoid gradient (r), and time constants (τ_b).

To solve the convolution in Equation (2), both $g(v(t))$ and $h_m(t)$ are transformed into the

Laplace domain

$$G(V(s)) = \frac{g_{\max}}{1 + \exp(r(V(s) - v_0))} \quad (4)$$

$$H_b(s) = \frac{d}{ds} \left(-\frac{G_b(s)}{\tau_b} \left(\frac{1}{s + \frac{1}{\tau_b}} \right) \right) \quad (5)$$

$$H_b(s) = \frac{G_b(s)}{\tau_b} \left(\frac{1}{s + \frac{1}{\tau_b}} \right)^2. \quad (6)$$

It is clear here that the sigmoid function has no functional dependence on time; therefore, the output of the sigmoid will be assumed to be an input firing rate ($u_b(t)$) where the time dependence is caused by the time varying membrane potential. The parameters $G_b(t)$ have an unknown functional dependence on time and are, therefore, assumed to be constant for this derivation. This simplifies the convolution equation to

$$G(V(s)) = U_b(s) \quad (7)$$

$$H_b(s) = \frac{G_b}{\tau_b} \left(\frac{1}{s + \frac{1}{\tau_b}} \right)^2 \quad (8)$$

$$V_b(s) = \frac{G_b U_b(s)}{\tau_b} \left(\frac{1}{s + \frac{1}{\tau_b}} \right)^2. \quad (9)$$

Using Equation (9), the membrane potential $v_b(t)$ can be described as a second order differential equation as follows

$$V_b(s) = \frac{G_b U_b(s)}{\tau_b} \left(\frac{1}{s^2 + \frac{2s}{\tau_b} + \frac{1}{\tau_b^2}} \right) \quad (10)$$

$$V_b(s) \left(s^2 + \frac{2s}{\tau_b} + \frac{1}{\tau_b^2} \right) = \frac{G_b(s) U_b(s)}{\tau_b}. \quad (11)$$

Taking the inverse Laplace transform of Equation (11) results in

$$\frac{d}{dt^2} v_b(t) + \frac{d}{dt} \left(\frac{2 * v_b(t)}{\tau_b} \right) + \frac{v_b(t)}{\tau_b^2} = \frac{G_b(t) u_b(t)}{\tau_b} \quad (12)$$

$$\frac{d}{dt^2} v_b(t) = \frac{G_b(t) u_b(t)}{\tau_b} - \frac{d}{dt} \left(\frac{2 * v_b(t)}{\tau_b^2} \right) - \frac{v_b(t)}{\tau_b^2}. \quad (13)$$

A dummy variable, $z(t)$, is defined such that Equation (13) can be described as two differential

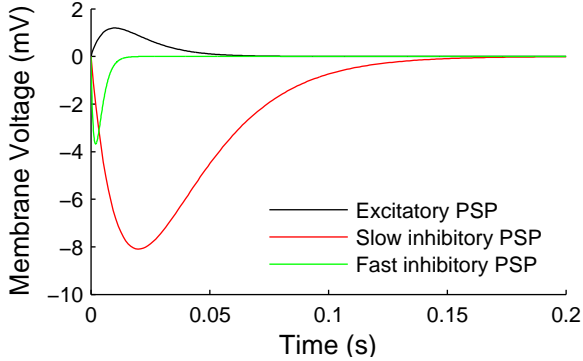


Figure 2: Impulse response of the firing rate to aggregate membrane potential function. The time constants and synaptic gains used for this figure correspond to that of background EEG (Wendling et al., 2002). The peaks of each response occur at time τ_b and the maximum membrane potential is $\exp(-1)G_b$, where b is replaced by p, s and f for excitatory, and slow and fast inhibitory time constants and gains, respectively. The inhibitory populations response is shown as negative, as this is its net effect on the system.

equations,

$$\frac{d}{dt}v_b(t) = \dot{v}_b(t) \quad (14)$$

$$\frac{d}{dt^2}v_b(t) = \ddot{z}_b(t) \quad (15)$$

$$\dot{v}_b(t) = z_b(t) \quad (16)$$

$$\ddot{z}_b(t) = \frac{G_b(t)}{\tau_b} n_b u_b(t) - 2 \frac{z_b(t)}{\tau_b} - \frac{v_b(t)}{\tau_b^2}. \quad (17)$$

Here $v_b(t)$ is the average membrane potential and $z_b(t)$ is its derivative. $G_b(t)$ and τ_b are the specific neural populations synaptic gain and time constant. Lastly, $u_b(t)$ is the firing rate to the specific neural population considered and n_b is a constant used to describe connectivity. The term n_b is a consequence of the model simplification, and its derivation is demonstrated in appendix 6.

Full mathematical description of the model Using Equations (16)-(17) and observing that each synapse of the model (totaling 8), shown in figure 1 requires two differential equations, the number of equations expected would be sixteen. However, this model can be simplified, see Ap-

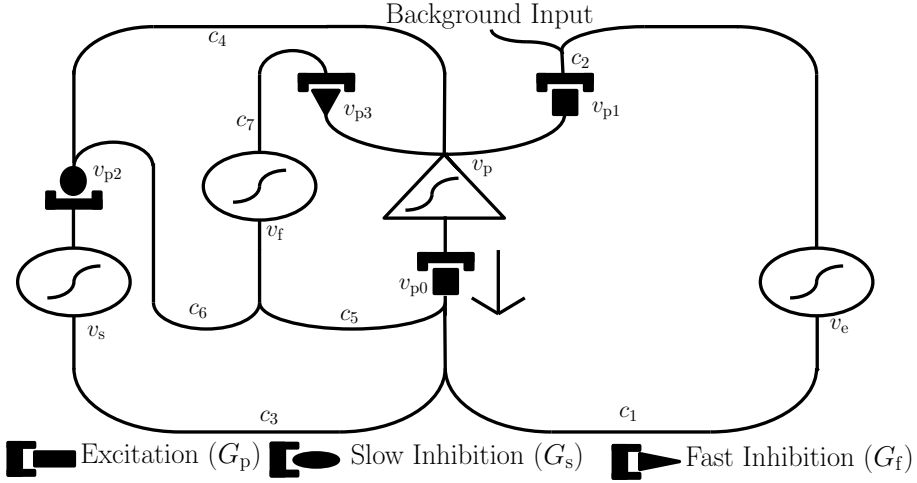


Figure 3: Simplified graphical description of the Wendling model.

pendix 6, (Figure 3) to a set of eight stochastic differential equations:

$$dv_{p0}(t) = z_{p0}(t)dt \quad (18)$$

$$dz_{p0}(t) = \left(\frac{G_p(t)}{\tau_p} n_p g(v_p(t)) - 2 \frac{z_{p0}(t)}{\tau_p} - \frac{v_{p0}(t)}{\tau_p^2} \right) dt \quad (19)$$

$$dv_{p1}(t) = z_{p1}(t)dt \quad (20)$$

$$dz_{p1}(t) = \left(\frac{G_e(t)}{\tau_e} (\mu + n_e g(v_e(t))) - 2 \frac{z_{p1}(t)}{\tau_e} - \frac{v_{p1}(t)}{\tau_e^2} \right) dt + \frac{G_e(t)}{\tau_e} \epsilon(t) dW \quad (21)$$

$$dv_{p2}(t) = z_{p2}(t)dt \quad (22)$$

$$dz_{p2}(t) = \left(\frac{G_s(t)}{\tau_s} n_s g(v_s(t)) - 2 \frac{z_{p2}(t)}{\tau_s} - \frac{v_{p2}(t)}{\tau_s^2} \right) dt \quad (23)$$

$$dv_{p3}(t) = z_{p3}(t)dt \quad (24)$$

$$dz_{p3}(t) = \left(\frac{G_f(t)}{\tau_f} n_f g(v_f(t)) - 2 \frac{z_{p3}(t)}{\tau_f} - \frac{v_{p3}(t)}{\tau_f^2} \right) dt. \quad (25)$$

In these equations dW represents a Wiener process and is required as $\epsilon(t) \sim N(0, \sigma)$, where σ and μ (Eq. (21)) describe the mean and variance of the stochastic model input, respectively. Further, $v_{p0-3}(t)$ represent the membrane potential produced by a specific populations synapse and $z_{p0-3}(t)$ their derivatives. The inputs to each neural population are specified by $v_b(t)$, and are the membrane potential of the specific population, where b takes the values of p, e, s and f representing pyramidal, excitatory, and slow and fast inhibitory populations, respectively. Therefore $v_p(t)$ is the output of

the model. All $v_b(t)$ can be described in terms of $v_{p0-3}(t)$ as follows

$$v_p(t) = v_{p1}(t) - c_4 v_{p2}(t) - v_{p3}(t) \quad (26)$$

$$v_e(t) = c_1 v_{p0}(t) \quad (27)$$

$$v_s(t) = c_3 v_{p0}(t) \quad (28)$$

$$v_f(t) = c_5 v_{p0}(t) - c_6 v_{p2}(t), \quad (29)$$

where c_1 , c_3 and c_5 represent the connectivity strength from pyramidal to excitatory, slow inhibitory and fast inhibitory populations, respectively. The last two connectivity terms, c_4 and c_6 , represent the connectivity strength from the slow inhibitory to the excitatory and fast inhibitory populations, respectively. Finally, all n_b can be defined as connectivity constants:

$$n_p = 1 \quad (30)$$

$$n_e = c_2 \quad (31)$$

$$n_s = 1 \quad (32)$$

$$n_f = c_7, \quad (33)$$

where c_2 and c_7 represent the connectivity strength from excitatory and fast inhibitory populations to the pyramidal population.

Simulation of model This set of continuous stochastic differential equations is discretised using Euler-Mariyama's method [ref](#), to simulate EEG

$$v_{p0,k+1} = v_{p0,k} + T z_{p0,k} \quad (34)$$

$$z_{p0,k+1} = z_{p0,k} + T \left(\frac{G_{p,k}}{\tau_p} n_p g(v_{p,k}) - 2 \frac{z_{p0,k}}{\tau_p} - \frac{v_{p0,k}}{\tau_p^2} \right) \quad (35)$$

$$v_{p1,k+1} = v_{p1,k} + T z_{p1,k} \quad (36)$$

$$z_{p1,k+1} = z_{p1,k} + T \left(\frac{G_{e,k}}{\tau_e} (\mu + n_e g(v_{e,k})) - 2 \frac{z_{p1,k}}{\tau_e} - \frac{v_{p1,k}}{\tau_e^2} \right) + \sqrt{T} \frac{G_{e,k}}{\tau_e} \epsilon_t \quad (37)$$

$$v_{p2,k+1} = v_{p2,k} + T z_{p2,k} \quad (38)$$

$$z_{p2,k+1} = z_{p2,k} + T \left(\frac{G_{s,k}}{\tau_s} n_s g(v_{s,k}) - 2 \frac{z_{p2,k}}{\tau_s} - \frac{v_{p2,k}}{\tau_s^2} \right) \quad (39)$$

$$v_{p3,k+1} = v_{p3,k} + T z_{p3,k} \quad (40)$$

$$z_{p3,k+1} = z_{p3,k} + T \left(\frac{G_{f,k}}{\tau_f} n_f g(v_{f,k}) - 2 \frac{z_{p3,k}}{\tau_f} - \frac{v_{p3,k}}{\tau_f^2} \right), \quad (41)$$

where k represents the current sample and T is the period between them. The static parameter

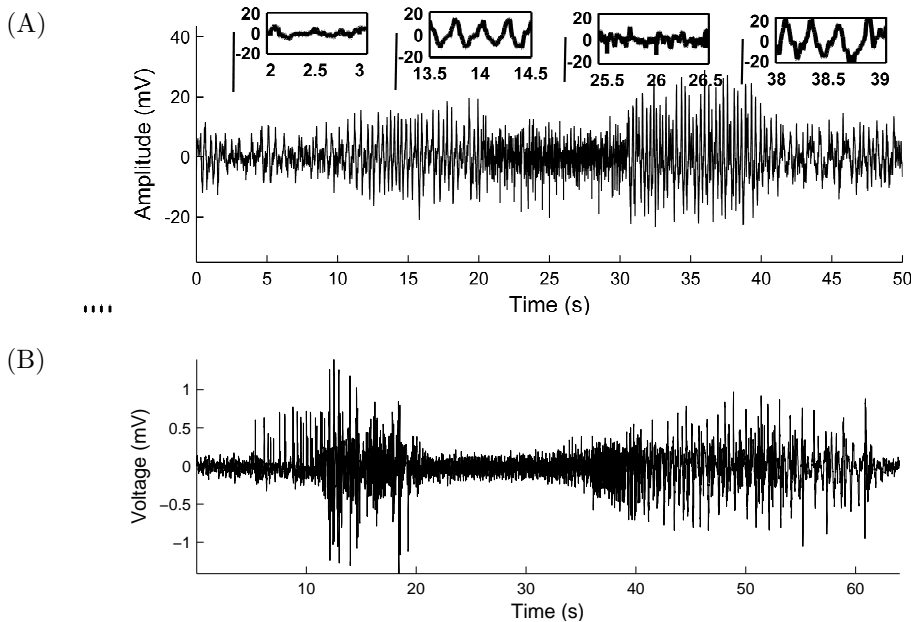


Figure 4: Simulated seizure using the Wendling model compared to a seizure recorded from an *in vivo* model of epilepsy.. (a) Here four different sets of synaptic gains are used to simulate the seizure. Four types of neural activity are demonstrated in this figure: background EEG (1-10s), interictal (11-20s), low voltage high frequency (21-30s) and seizure (31-40s). The last ten seconds shows background data again. Four insets are demonstrated in the figure each corresponding to a different type of activity. The insets in order from left to right show: background, interictal, low voltage high frequency and seizure activity. (b) Tetanus toxin focal seizure data, where four types of activity are demonstrated: background(1-5s), interictal (6-20s), low voltage high frequency (21-35s) and seizure (36-60s).

Table 1: Static Model Parameters (Wendling et al., 2002). Here p, e, s and f represent populations of pyramidal neurons and excitatory, and slow and fast inhibitory interneurons, respectively.

MODEL PARAMETER	PHYSICAL DESCRIPTION	VALUE	UNITS
τ_p	Time constant for pyramidal neurons	100	s^{-1}
τ_e	Time constant for excitatory neurons	100	s^{-1}
τ_s	Time constant for slow inhibitory neurons	35	s^{-1}
τ_f	Time constant for fast inhibitory neurons	500	s^{-1}
c	Connectivity constant	135	NA
c_1	Connectivity constant (p - e)	c	NA
c_2	Connectivity constant (e - p)	$0.8c$	NA
c_3	Connectivity constant (p - s)	$0.25c$	NA
c_4	Connectivity constant (s - p)	$0.25c$	NA
c_5	Connectivity constant (p - f)	$0.3c$	NA
c_6	Connectivity constant (s - f)	$0.1c$	NA
c_7	Connectivity constant (f - p)	$0.8c$	NA
g_{max}	Maximum firing rate	5	Hz
v_0	PSP for which 50% firing rate is achieved	6	mV^{-1}
r	Gradient of sigmoid function	0.56	NA
f_{max}	Maximum input firing rate	150	Hz
f_{min}	Minimum input firing rate	30	Hz
μ	Input mean firing rate	90	Hz
σ	Variance of input firing rate	15	Hz

values are shown in Table 1. The variance of the input, σ , is specified such that 99.7% of realisations drawn from the Gaussian distribution fall within the specified maximum and minimum firing rate. For the cases where the realisations from the Gaussian distribution are not contained within the limits specified, the specific sample of interest is redrawn from the same Gaussian distribution until the firing rate falls within the specified range. In Table 1, the parameters $G_{p,k}$, $G_{e,k}$, $G_{s,k}$ and $G_{f,k}$ are not specified as these parameters will vary for different simulations. However, for this simulation, it is assumed that

$$G_{p,k} = G_{e,k}. \quad (42)$$

This assumption can be made as the excitatory population in this model specifies recurrent connections between pyramidal neurons.

2.2 Estimation

Generic description on a nonlinear system A generic system is defined where

$$\dot{\mathbf{x}}(t) = \mathbf{A}(\mathbf{x}(t), \theta(t)) + \mathbf{B}(\mathbf{u}(t)) + \mathbf{n}(t) \quad (43)$$

$$\mathbf{y}(t) = \mathbf{C}(\mathbf{x}(t)) + \mathbf{D}(\mathbf{u}(t)) + \mathbf{r}(t), \quad (44)$$

where boldface indicates a matrix or vector. Here, $\mathbf{x}(t)$ is the state vector and $\dot{\mathbf{x}}(t)$ is its derivative, where

$$\dot{\mathbf{x}}(t) = \begin{bmatrix} \dot{x}_1(t) \\ \vdots \\ \dot{x}_n(t) \end{bmatrix}.$$

\mathbf{A} and \mathbf{B} are the state and input functions, respectively and $\mathbf{u}(t)$ is the input to the model. \mathbf{C} and \mathbf{D} are the output and input-to-output functions, respectively. The output of the model is $\mathbf{y}(t)$ with $\mathbf{n}(t)$ the model uncertainty, and $\mathbf{r}(t)$ the observation noise. Here, $\mathbf{n}(t)$ takes into account that the model is not a perfect descriptor of the modeled system as well as accounting for unknown inputs to the system, and $\mathbf{r}(t)$ describes the maximum amplitude of the noise in the observations. Both $\mathbf{n}(t)$ and $\mathbf{r}(t)$ are zero mean Gaussian distributed with a system dependant variance. The assumption of Gaussian distribution is only valid when the number of samples for the estimation procedure is large (central limit theorem ref). In particular, the sampling rate needs to be much greater than the maximum frequency that the model dynamics describes. This is often referred to as an oversampled system ref.

Introduction to the UKF Estimation algorithms usually estimate the model states, $\mathbf{x}(t)$, given some observation, $\mathbf{y}(t)$. One method that is often used for estimating linear systems is the Kalman filter. The Kalman filter consists of two steps: prediction and correction. In the prediction step, model states are propagated through the system and are used to determine the expected value of the states at the next time step. Using a first order Euler-Maruyama method, this can be described by

$$\mathbf{x}_{k+1}^- = \mathbf{x}_k + T(\mathbf{Ax}_k + \mathbf{Bu}_k) + \sqrt{T}\mathbf{n}_k \quad (45)$$

$$\mathbf{y}_{k+1}^- = \mathbf{y}_k + T(\mathbf{Cy}_k + \mathbf{Du}_k) + \sqrt{T}\mathbf{r}_k, \quad (46)$$

where the subscript in \mathbf{x}_k^- is used to indicate the current sample and T is the sampling period. The stochastic variables are $\mathbf{n}_k \sim N(0, \sigma_n)$ and $\mathbf{r}_k \sim N(0, \sigma_r)$, where σ_n and σ_r are the standard deviations for each respective noise process and $N(\cdot)$ is a Gaussian distribution. The superscript in \mathbf{x}_k^- is used to indicate that this estimate is a prediction that has not yet been corrected by the current observation. Performing this kind of prediction for a nonlinear system would be inaccurate as the propagation of states like this in a system would require the assumption that the maximum error in the states remains constant for all time. However, in a nonlinear system this is not true, as a state's error can change from one prediction to the next. In particular, if the original state estimate is incorrect in a nonlinear system it is possible that the error can increase in the next iteration of the estimation procedure. In order to account for this error, or the altering of state covariance, an unscented filter is used in the prediction step for nonlinear systems. The advantage of an unscented filter over local linearisation techniques is that speed is improved and discontinuities can be handled.

The unscented filter The unscented filter is completely described by a state's mean and covariance such that:

$$\mathcal{X}_n = \bar{\mathbf{x}}_k + (\sqrt{\kappa + D_x \mathbf{P}_{\mathbf{xx},k}})_n \quad n = 1, \dots, D_x \quad (47)$$

$$\mathcal{X}_{n+D_x} = \bar{\mathbf{x}}_k - (\sqrt{\kappa + D_x \mathbf{P}_{\mathbf{xx},k}})_n \quad n = 1, \dots, D_x, \quad (48)$$

$$\mathcal{Y}_n = \bar{\mathbf{y}}_k + (\sqrt{\kappa + D_y \mathbf{P}_{\mathbf{yy},k}})_n \quad n = 1, \dots, D_y \quad (49)$$

$$\mathcal{Y}_{n+D_y} = \bar{\mathbf{y}}_k - (\sqrt{\kappa + D_y \mathbf{P}_{\mathbf{yy},k}})_n \quad n = 1, \dots, D_y, \quad (50)$$

where $\bar{\mathbf{x}}_k$ and $\bar{\mathbf{y}}_k$ are the current state estimate and observation. $(\sqrt{\cdot})_n$ denotes the n th row of the matrix square root. D_x and D_y indicate the number of states in the system and the number of observations. Covariance matrices, $\mathbf{P}_{\mathbf{xx},k}$ and $\mathbf{P}_{\mathbf{yy},k}$, are the expected error of the current state and observation. The points \mathcal{X} are called sigma points and represent the states one standard deviation away for the estimated mean. The term κ is a predefined constant, which determines the relative effect of the propagation of the

mean. If κ is equal to zero then the system mean is not propagated as a sigma point. However, if κ is greater than zero then

$$\mathcal{X}_0 = \bar{\mathbf{x}}_k. \quad (51)$$

Therefore, $2D_x$ sigma points are assigned when κ is zero and $2D_x+1$ sigma points are assigned when it is greater than zero. The sigma points are propagated through the system in order to update the expectation about the state mean and error:

$$\mathcal{X}_{n,k+1} = \mathcal{X}_{n,k} + T(\mathbf{A}(\mathcal{X}_{n,k}) + \mathbf{B}(\mathbf{u}_k)) + \sqrt{T}n_k \quad (52)$$

$$\bar{\mathbf{x}}_{k+1}^- = \frac{1}{2D_x + \kappa} \sum_{n=1}^{2D_x} \mathcal{X}_{n,k+1} \quad (53)$$

$$\mathbf{P}_{xx,k+1}^- = \frac{1}{2D_x + \kappa} \sum_{n=1}^{2D_x} (\mathcal{X}_{n,k+1} - \bar{\mathbf{x}}_{k+1}^-)(\mathcal{X}_{n,k+1} - \bar{\mathbf{x}}_{k+1}^-)^\top + \mathbf{Q}. \quad (54)$$

$\bar{\mathbf{x}}_{k+1}^-$ and $\mathbf{P}_{xx,k+1}^-$ are the predictions for the state and state covariance matrices. The negative superscript is used to indicate an uncorrected prediction. The term \mathbf{Q} is the expectation of the model error n_k and $(\cdot)^\top$ indicates the transpose. It is now possible to make a prediction about the observation at sample $k+1$ by propagating the sigma points through Equation (46)

$$\mathcal{Y}_{n,k+1} = \mathcal{Y}_{n,k} + T(\mathbf{C}(\mathcal{X}_{n,k+1}) + \mathbf{D}(\mathbf{u}_k)) + \sqrt{T}\mathbf{r}_k \quad (55)$$

$$\bar{\mathbf{y}}_{k+1}^- = \frac{1}{2D_x + \kappa} \sum_{n=1}^{2D_x} \mathcal{Y}_{n,k+1} \quad (56)$$

$$\mathbf{P}_{xy,k+1}^- = \frac{1}{2D_x + \kappa} \sum_{n=1}^{2D_x} (\mathcal{X}_{n,k+1} - \bar{\mathbf{x}}_{k+1}^-)(\mathcal{Y}_{n,k+1} - \bar{\mathbf{y}}_{k+1}^-)^\top \quad (57)$$

$$\mathbf{P}_{yy,k+1}^- = \frac{1}{2D_x + \kappa} \sum_{n=1}^{2D_x} (\mathcal{Y}_{n,k+1} - \bar{\mathbf{y}}_{k+1}^-)(\mathcal{Y}_{n,k+1} - \bar{\mathbf{y}}_{k+1}^-)^\top + \mathbf{R}, \quad (58)$$

where $\bar{\mathbf{y}}_{k+1}^-$ and $\mathbf{P}_{yy,k+1}^-$ are the predictions for the model output and its covariance, respectively. $\mathbf{P}_{xy,k+1}^-$ is the covariance matrix of the states and observations and \mathbf{R} is the expectation of the observation error \mathbf{r}_k .

How states are predicted using the unscented transform The predictions of the states, $\bar{\mathbf{x}}_{k+1}^-$, and observations, $\bar{\mathbf{y}}_{k+1}^-$, now need to be corrected based on the observations. This is achieved by determining the Kalman gain and updating the predictions based on the current observation:

$$\mathbf{K} = \mathbf{P}_{xy,k+1}^-(\mathbf{P}_{yy,k+1}^-)^{-1} \quad (59)$$

$$\bar{\mathbf{x}}_{k+1} = \bar{\mathbf{x}}_{k+1}^- + \mathbf{K}(\mathbf{y}_{k+1} - \bar{\mathbf{y}}_{k+1}^-) \quad (60)$$

$$\mathbf{P}_{xx,k+1} = \mathbf{P}_{xx,k+1}^- - \mathbf{K}(\mathbf{P}_{xy,k+1}^-)^\top, \quad (61)$$

where \mathbf{y}_k is the observation, $\bar{\mathbf{x}}_{k+1}$ is the corrected estimate of the state and $\mathbf{P}_{xx,k+1}$ is the estimate of its error. This set of equations describes the UKF and how it can be used to estimate states. However, for this study, estimation of states and parameters is required (dual estimation).

Definition of slow state matrix and its dynamics The parameters that are being estimated are $G_{p,k}$, $G_{e,k}$, $G_{s,k}$ and $G_{f,k}$, where it is assumed that

$$G_{p,k} = G_{e,k}. \quad (62)$$

Therefore, three parameters need to be estimated, and a parameter matrix is defined

$$\theta_k = \begin{bmatrix} G_{p,k} \\ G_{s,k} \\ G_{f,k} \end{bmatrix}.$$

The original state matrix is then augmented with the parameter matrix

$$\mathbf{x}_k = \begin{bmatrix} \mathbf{x}_k \\ \theta_k \end{bmatrix}.$$

The change in model parameters occurs at a longer time scale than the model states. Therefore, for convenience, the model states and parameters are referred to as fast and slow states. The next issue to consider is the description of the dynamics for the slow states. Due to the prediction correction steps of the unscented Kalman filter these slow states can be assigned trivial dynamics such that

$$\theta_{k+1} = \theta_k + \eta_k \quad (63)$$

$$E(\theta_{k+1}) = \theta_k \quad (64)$$

$$P_{\theta\theta,k+1} = \Psi, \quad (65)$$

where $E(\cdot)$ is the expectation function and $\eta_k \sim N(0, \sigma)$.

Intialisation of UKF for stationary parameters When initialising the unscented Kalman filter the model uncertainty and initialisation standard deviation for each state needs to be specified. To determine the accuracy of the model when estimating fast states, initial estimations are performed under the assumption that the model's slow states are stationary. Assuming that the model slow states are stationary allows for the uncertainty in these states to remain low. This uncertainty characterises possible model inaccuracy, and also allows the slow state to slowly vary until they converges to their true values. Standard deviations in the estimation description are described such that one standard deviation from the midpoint of the specified slow states range encompasses all possible values for the particular state. Further, the uncertainty of states directly affected by the stochastic model input is increased to account for the unpredictable nature of this signal when simulating. This is required as a stochastic process cannot be estimated accurately.

Due to the stochastic model input, it is non-trivial to determine the maximum limit of the physiological range describing the fast states. Therefore, numerous simulations are performed and the resulting mean and standard deviation for each state is used as the initial mean and standard deviation for estimation:

$$v_{b,0} = \frac{1}{n} \sum_{i=1}^n E(v_{i,b,k}), \quad (66)$$

where n indicates the number of simulations performed and $v_{b,0}$ and $E(v_{b,k,i})$ indicate the expected value of the initialised fast states and the expected value of each simulation, respectively. For the standard deviation, the average over multiple simulations for a normal distribution can be determined by

$$\sigma_{b,0}^2 = \frac{1}{n-1} \sum_{i=1}^n \sigma_{b,k}^2, \quad (67)$$

where $\sigma_{b,0}^2$ and $\sigma_{b,k}^2$ are the variances of the initial guess and of each state's simulation results, respectively.

Next the assignment of the mean and covariance of the slow states is considered. For this calculation it is assumed that all possible values of the slow states are equally probable. The range of these slow states is infinite; however, there is a physiological bound on their values (Wendling et al., 2002). These bounds

will be used and are defined as $\theta_{b,max}$ and $\theta_{b,min}$. The mean and covariance of the slow states are

$$\bar{\theta}_{b,0} = \frac{\theta_{b,max} + \theta_{b,min}}{2} \quad (68)$$

$$P_{\theta\theta,0} = (\bar{\theta}_{b,0} - \theta_{b,min})^2. \quad (69)$$

Initialisation of UKF for varying parameters When estimating slow states that vary within a single simulation, the uncertainty assigned to these parameters is increased. This increase in uncertainty guarantees that the estimation procedure will not converge to a specific slow state and remain there, but instead will track it as it varies.

Estimation of model input mean Finally, estimation of the stochastic input's mean to the neural mass is considered. Here it is assumed that the model input mean is varying slowly. By doing so the input mean can be augmented to the state matrix and assigned trivial dynamics. With the physiological bounds on the input specific by Wendling et al. (2002), the initial mean and standard deviation of the input can be defined by equations 68-69.

Robustness test The performance of the estimation procedure is determined. Initially, only estimation of fast states is considered. This is then developed to the full estimation procedure where all model parameters and the input mean are estimated. The estimation procedure is then tested under numerous observation noise conditions, and with varying levels of error in the initialisation of states.

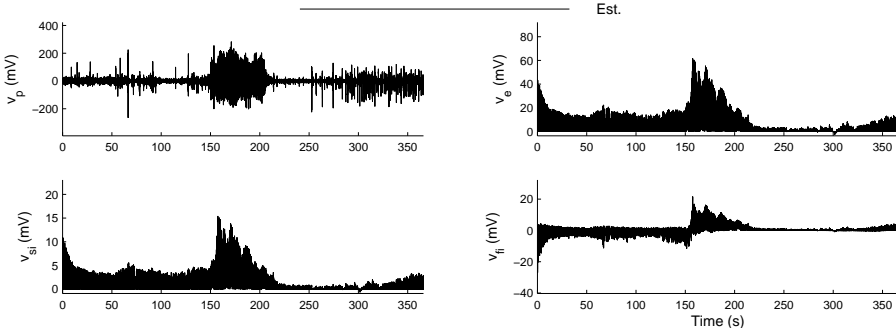


Figure 5: Animal 5 Seizure 1 Population potentials Channel 1. Black: Estimated. In this figure seizure begins at 150 seconds and terminates 150 seconds prior to the end of the time series. Here v_p , v_e , v_{si} and v_{hi} represent the membrane potentials of the pyramidal, excitatory (spiny stellate), slow inhibitory (peri-dendritic) and fast inhibitory (peri-somatic) populations, respectively.

3 Results

For this study recording are made from four electrodes in an *in vivo* model of focal epilepsy. Two electrodes are placed within the hippocampus (Channel 1 and Channel 2) - which is the seizure focus for this *in vivo* model - and the other two are placed on the cortex (Channel 3 and Channel 4). The data recorded from these electrodes is used as the observations for a statistical inference method, with a specific neural mass model. In this case we consider the Wendling model which has been shown to be a coarse description of hippocampal physiology, and can mimic the phenomena observed in hippocampal EEG.

In this document two different animals are considered on the same day. Animal 5 and 6 had 10 and 6 seizures respectively on the considered day. Here we show a subset of these results to demonstrate the fidelity of the statistical inference method. All EEG shown in this document contains 150 seconds of pre- and post-ictal data.

3.1 Animal 5 Seizure 1 13/03/09

This seizure lasted 60 seconds, so for all figures the seizure start is at 150 seconds and ends at 210 seconds. The seizure was **Convulsive or non convulsive**.

In figure 5 the estimated membrane potentials of all populations is demonstrated. The membrane potential v_p is the estimated membrane potential of the pyramidal population, which is also the output of the model. This is very similar to the actual recorded data with one major difference: the Kalman filter has removed observation noise.

The estimated spiny stellate cells membrane potential increases at seizure initiation, and slowly decreases until seizure termination. During the pre-ictal period the estimated amplitude of the spiny stellate fluctuates randomly. Post-ictal the membrane potential of the spiny stellate cells steadily increases until it returns to normal. A similar trend is observed in the peri-dendritic inhibitory population, and the peri-somatic inhibitory population. However, the peri-somatic membrane potential is negative pre-ictal and positive during seizure and post-ictal.

In figure 6 the estimated model states are demonstrated.

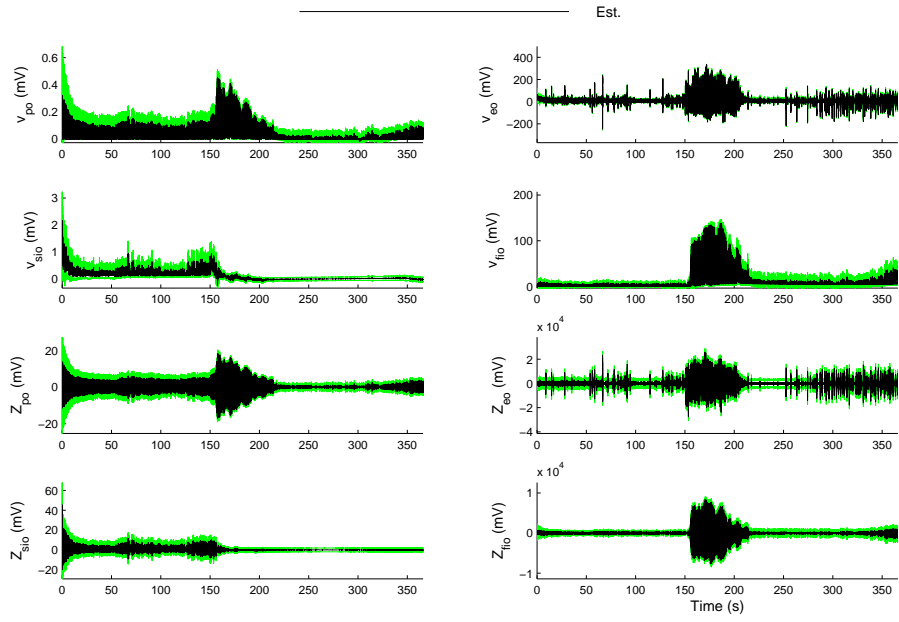


Figure 6: Animal 5 Seizure 1 Model States Channel 1. Black, green are the estimated results and its expected error, respectively. In this figure seizure begins at 150 seconds and terminates 150 seconds prior to the end of the time series. Here v and z indicate the effective membrane potential that the specified population outputs - i.e. the net effect of the considered population on all populations it directly affects - and the derivative of this membrane potential, respectively.

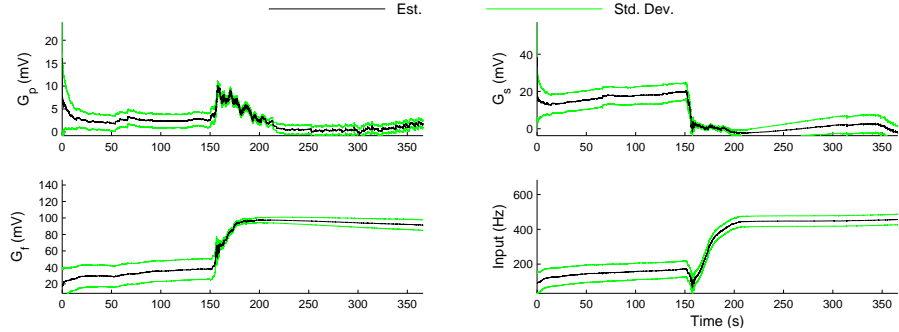


Figure 7: Animal 5 Seizure 1 Model Parameters Channel 1. Black, green are the estimated results and its expected error, respectively. In this figure seizure begins at 150 seconds and terminates 150 seconds prior to the end of the time series.

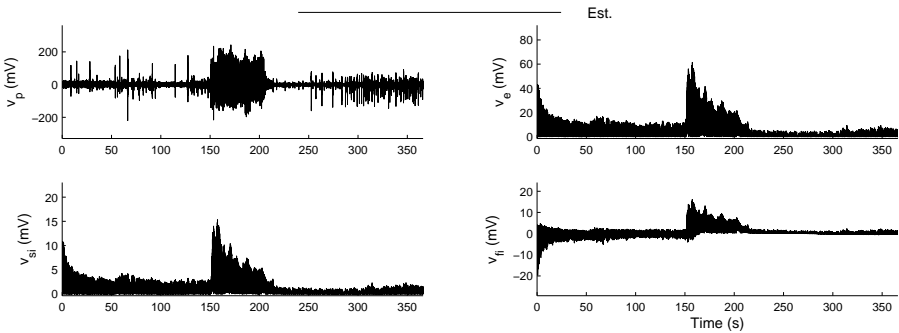


Figure 8: Animal 5 Seizure 1 Membrane Potentials Channel 2. Black: Estimated. In this figure seizure begins at 150 seconds and terminates 150 seconds prior to the end of the time series.

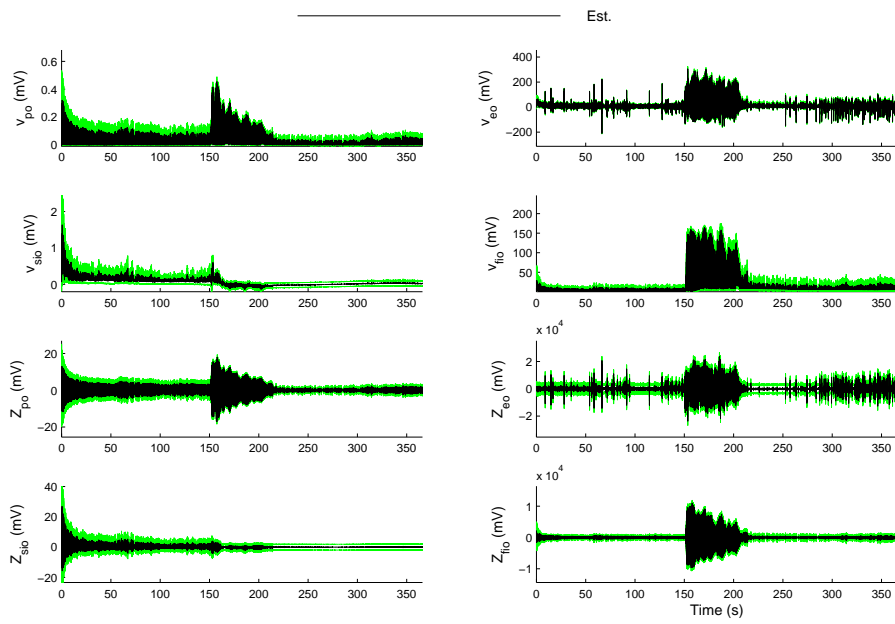


Figure 9: Animal 5 Seizure 1 Model States Channel 2. Black, green are the estimated results and its expected error, respectively. In this figure seizure begins at 150 seconds and terminates 150 seconds prior to the end of the time series.

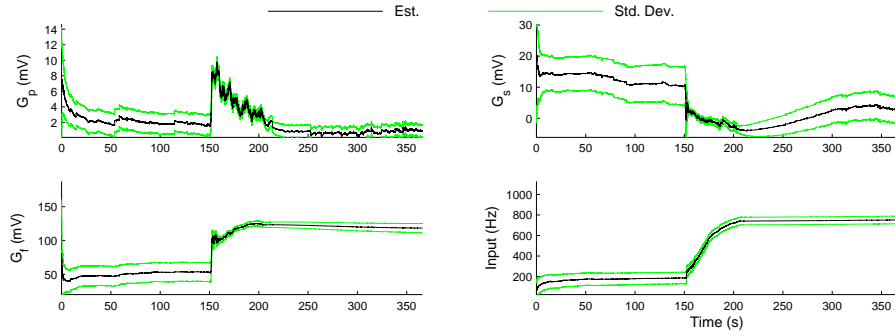


Figure 10: Animal 5 Seizure 1 Model Parameters Channel 2. Black, green are the estimated results and its expected error, respectively. In this figure seizure begins at 150 seconds and terminates 150 seconds prior to the end of the time series.

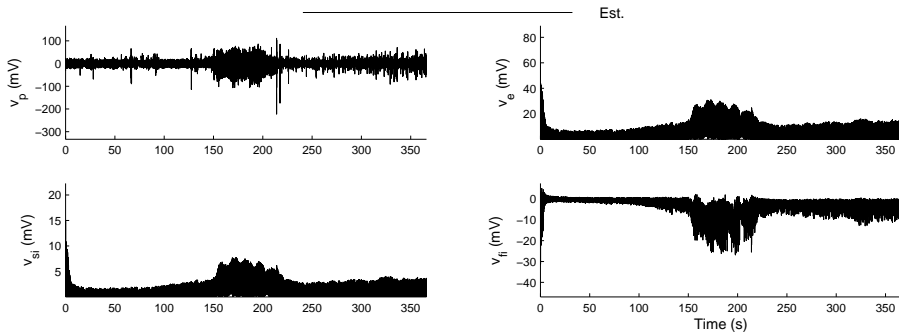


Figure 11: Animal 5 Seizure 1 Population potentials Channel 3. Black: Estimated. In this figure seizure begins at 150 seconds and terminates 150 seconds prior to the end of the time series.

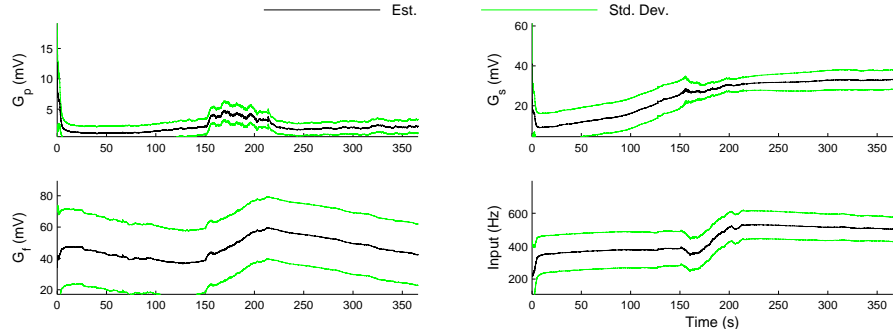


Figure 12: Animal 5 Seizure 1 Model Parameters Channel 3. Black, green are the estimated results and its expected error, respectively. In this figure seizure begins at 150 seconds and terminates 150 seconds prior to the end of the time series.

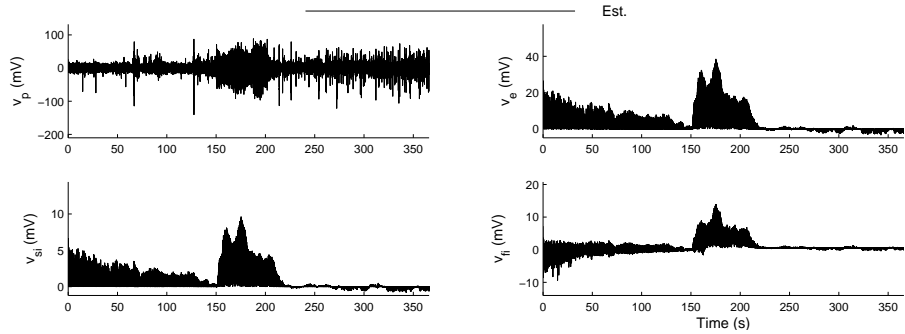


Figure 13: Animal 5 Seizure 1 Population potentials Channel 4. Black: Estimated. In this figure seizure begins at 150 seconds and terminates 150 seconds prior to the end of the time series.

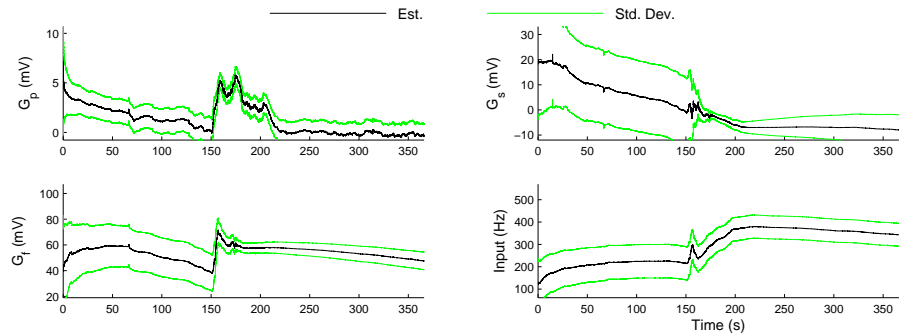


Figure 14: Animal 5 Seizure 1 Model Parameters Channel 4. Black, green are the estimated results and its expected error, respectively. In this figure seizure begins at 150 seconds and terminates 150 seconds prior to the end of the time series.

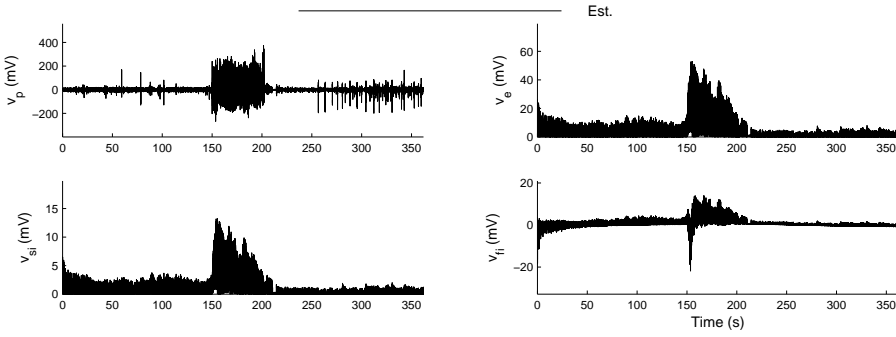


Figure 15: Animal 5 Seizure 2 Population potentials Channel 2. Black: Estimated. In this figure seizure begins at 150 seconds and terminates 150 seconds prior to the end of the time series.

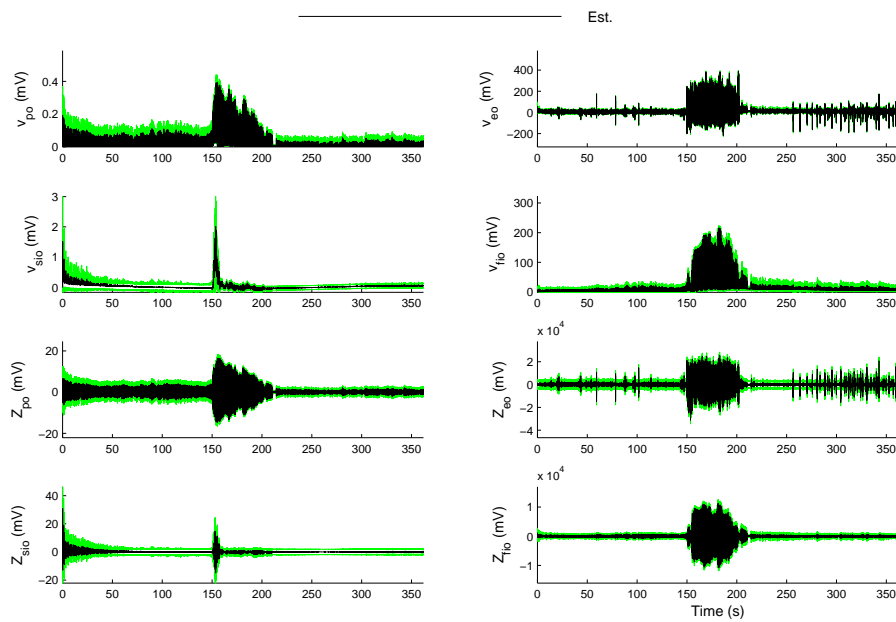


Figure 16: Animal 5 Seizure 2 Model States Channel 2. Black, green are the estimated results and its expected error, respectively. In this figure seizure begins at 150 seconds and terminates 150 seconds prior to the end of the time series.

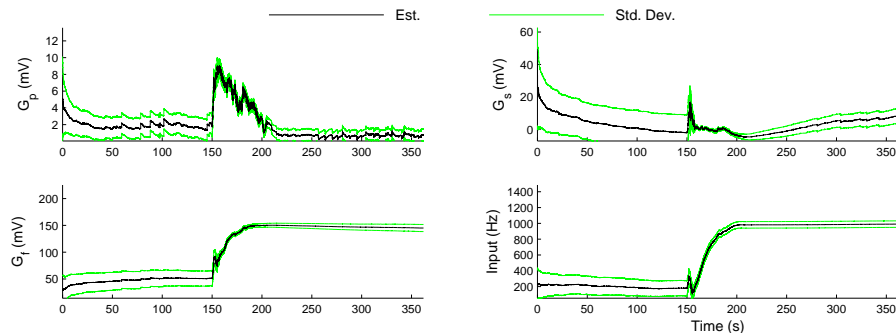


Figure 17: Animal 5 Seizure 2 Model Parameters Channel 2. Black, green are the estimated results and its expected error, respectively. In this figure seizure begins at 150 seconds and terminates 150 seconds prior to the end of the time series.

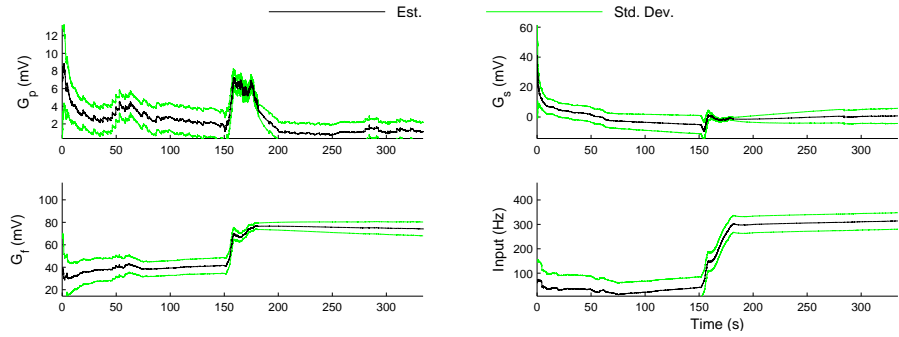


Figure 18: Animal 5 Seizure 3 Model Parameters Channel 2. Black, green are the estimated results and its expected error, respectively. In this figure seizure begins at 150 seconds and terminates 150 seconds prior to the end of the time series.

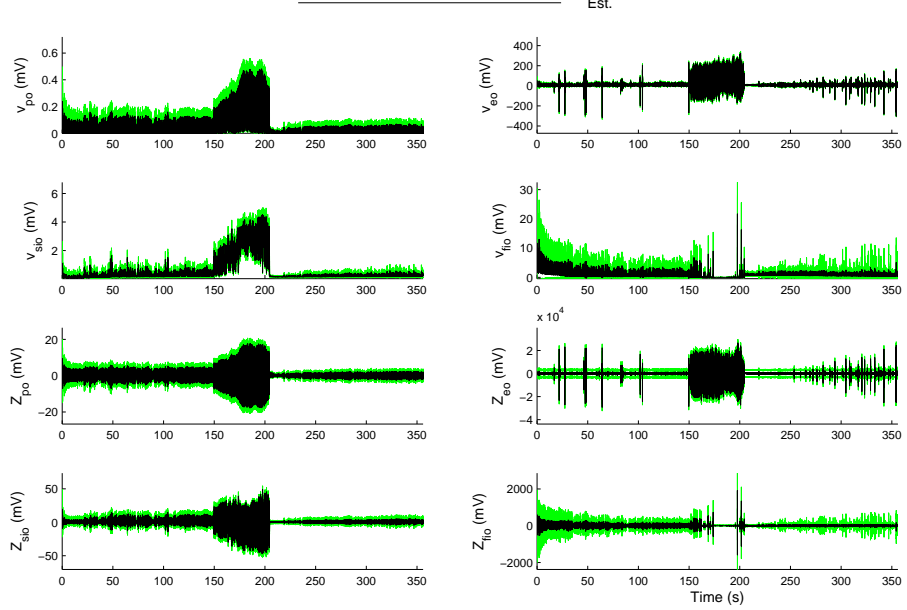


Figure 19: Animal 6 Seizure 1 Model States Channel 2. Black, green are the estimated results and its expected error, respectively. In this figure seizure begins at 150 seconds and terminates 150 seconds prior to the end of the time series.

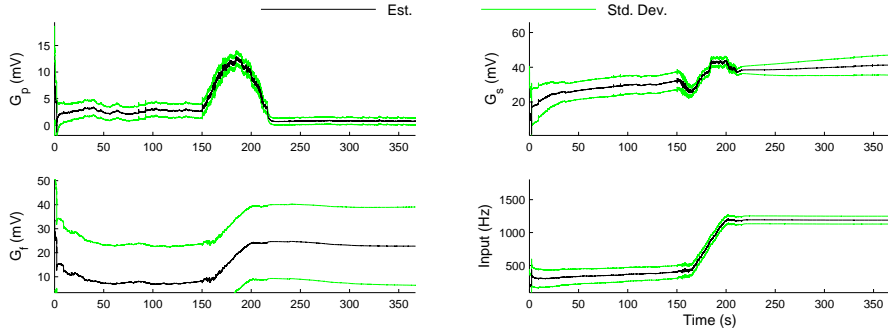


Figure 20: Animal 6 Seizure 2 Model Parameters Channel 2. Black, green are the estimated results and its expected error, respectively. In this figure seizure begins at 150 seconds and terminates 150 seconds prior to the end of the time series.

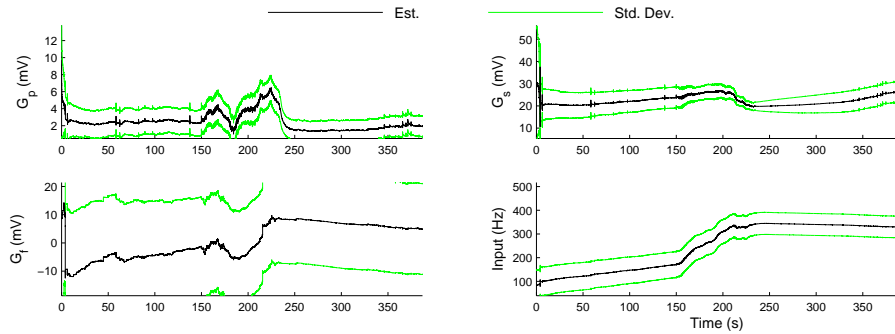


Figure 21: Animal 6 Seizure 3 Model Parameters Channel 2. Black, green are the estimated results and its expected error, respectively. In this figure seizure begins at 150 seconds and terminates 150 seconds prior to the end of the time series.

3.2 Animal 5 Seizure 2 13/03/09

3.3 Animal 5 Seizure3 13/03/09

3.4 Animal 6 Seizure1 13/03/09

3.5 Animal 6 Seizure2 13/03/09

3.6 Animal6 Seizure3 13/03/09

4 Discussion

Why estimation Epilepsy is a poorly understood disorder, and there is much uncertainty about the mechanisms involved in seizure generation. However, with computational models of neural activity getting more descriptive of physiology, it is becoming possible to gain insights into the underlying mechanism involved in observed electroencephalographic (EEG) recordings. However, models of EEG are highly non-linear, and standard estimation techniques cannot be used to approximate the physiological states from these models. In this paper, the application of the unscented Kalman filter to the Wendling model has been considered. From the results shown it is clear that this method is capable of estimating the slow states from this model.

Effect of stochastic input In figure ?? the estimation of excitatory synaptic gain is considered. From this image it is clear that this estimation does not converge to the true value of the parameter. However, consider the structure of the model (figure 1 where this synaptic gain acts on numerous signals to create the observations (v_p)). One of the inputs is the firing rate from other neural populations, which is stochastic. The stochastic nature of this input would result in variations in the simulated observations which cannot be directly incorporated into the estimation procedure. An attempt is made to reduce their effect on the estimation procedure by increasing the uncertainty in the model. However, if the uncertainty in the model is increased excessively the estimation procedure fails (figure ??). This is due to the structure of the Kalman filter which attempts to balance the amount of information received from the estimated model states and the observations, based on the certainty of each. Consider figure ?? where the observation noise is increased. This increase in noise leads to a decrease in the certainty in the measurements, which results in less variations in the estimate of the excitatory synaptic gain. This demonstrates that an increase in observation noise may benefit estimation up to a point.

Estimation of model parameters In figure ?? estimation of three model slow states is demonstrated. Here the excitatory gain still swings around its actual value. However, the estimate for the inhibitory synaptic gains converge to their true values. From this results, it is clear that the effect of the stochastic input on the model is filtered by the excitatory population, and the uncertainty in the estimation procedure can account for the small effect it has on the inhibitory slow states. This effect can be observed by noting that the stochastic input goes through an excitatory synapse before affecting the inhibitory populations. And when referring back to equation 9 it is clear that these synapses act as low pass filters, that is they reduce the effect of high frequency noise. The estimation of the input mean shown in figure ?? converges to its actual value. This input mean specifies the mean of the stochastic input, and should not be affected by the variance of the actual input.

Initialisation error Next the problem of initialisation error is considered. In figure ?? the model states are initialised randomly. The results show that if the parameter is distant from its actual value, the estimation procedure does not converge to the actual value of the slow states. This problem can be overcome by iteratively running the same estimation procedure but using different initial states drawn from a Gaussian distribution described in the methods section. Further, a criteria is assigned to the final estimate, that being that all final estimates should be within their specified physiological range. From figure ?? it is clear that although time consuming this procedure does eventually result in the convergence of the model slow states to their correct values.

Observation Noise If the noise in the observations is large the estimation procedure will fail. This effect is shown in figures ??-??. In figure ?? two of the model parameters seem to diverge, indicating that the model has been unable to track the changes occurring in the observations.

Parameters varying Lastly, and most importantly, the estimation of varying parameters is considered. In figure ?? it is shown that model parameters can be tracked even when they are varying within a single simulation. In figure ?? it is shown that the input mean can also be estimated during this procedure. Interestingly, the results from this procedure seem to indicate, that in this specific model, the slow inhibition synaptic gain is closely linked to the input mean, whereas the other model parameters do not seem to be affected by it. This result is interesting in light of studies where the input mean of the model is not

estimated, and observations of the synaptic gain of the slow inhibitory population are considered to be responsible for the change in dynamics (Wendling et al., 2005). It is worthwhile considering that the change in slow inhibition may be over or under-estimated if the input mean varies.

The results here have shown that the UKF is capable of estimating the synaptic gains and input mean of the Wendling model under numerous conditions. The insights gained from this estimation procedure may allow for better seizure prediction and detection. However, for on-line prediction of seizures (if this becomes possible) a method to initialise model parameters quickly and relatively accurately will need to be considered. Simplifying the model by linearising it and then using a linear Kalman filter may allow for the parameters to be initialised with some accuracy, and then the estimation can be switched to the UKF for better accuracy. Using these kinds of techniques will not only help in the prediction and detection of seizure, but possibly in the treatment of neurological disorders. The effect of treatment on slow states can be compared to the effect of, for example, seizure on these states. Treatments can then be tailored to individual patients to force slow states farther away from the state subspace where the disorders clinical manifestations are observed.

5 Conclusion

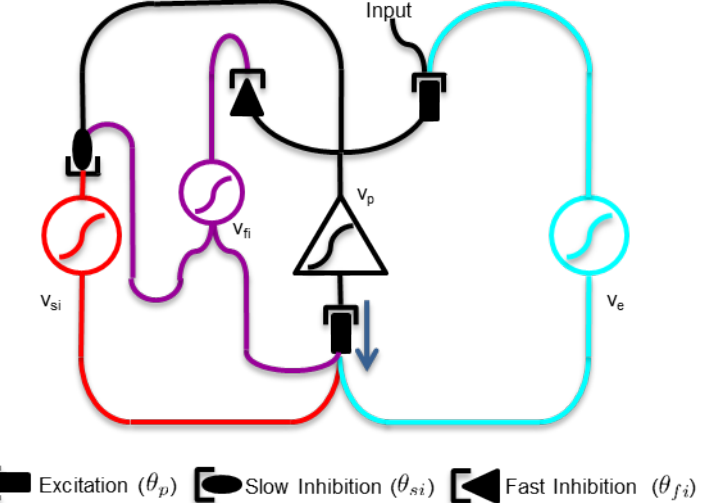


Figure 22: Graphical Description of the Wendling model (Minimised). Membrane potentials are shown and named v_b where b is p, e, fi and si for pyramidal, excitatory and slow and fast inhibitory populations, respectively. The synaptic gains of each population are specified by θ_m where m is defined in the same manner as the membrane potentials and $\theta_p = \theta_e$. Each triangle and circle indicates a neural population. In particular, the triangle shape indicates the pyramidal population and the circle shapes represent interneurons. The triangles and circles model the action of the soma for the neural populations, and convert membrane potentials to firing rates. The synapses convert the firing rates to membrane potentials. Lastly, each line indicates a neural connection, which is specified by a connectivity constant.

6 Appendix

The reduction of the Wendling model is based on the principles of linear superposition. First notice that each synapse is a linear lowpass filter (equation 9). In figure 1 there are eight such synapse. However, notice that numerous of these synapse have identical synaptic gains, and are connected by different connectivity constants. Given that for a linear system it is known that

$$f(a\mathbf{x}) = af(\mathbf{x}), \quad (70)$$

where $f(\cdot)$ is an arbitrary function, and a is a constant. Therefore, the model can be simplified by moving the synapse closer to the respective populations. The result of this process is demonstrated in figure 22.

Now consider the full set of original model equations that would be required to specify figure 1

$$dv_{po*}(t) = z_{po*}(t)dt \quad (71)$$

$$dz_{po*}(t) = \left(\frac{\theta_p(t)}{\tau_p} c_1 g(v_p(t)) - 2 \frac{z_{po*}(t)}{\tau_p} - \frac{v_{po*}(t)}{\tau_p^2} \right) dt \quad (72)$$

$$dv_{p1*}(t) = z_{p1*}(t)dt \quad (73)$$

$$dz_{p1*}(t) = \left(\frac{\theta_p(t)}{\tau_p} c_3 g(v_p(t)) - 2 \frac{z_{p1*}(t)}{\tau_p} - \frac{v_{p1*}(t)}{\tau_p^2} \right) dt \quad (74)$$

$$dv_{p2*}(t) = z_{p2*}(t)dt \quad (75)$$

$$dz_{p2*}(t) = \left(\frac{\theta_p(t)}{\tau_p} c_5 g(v_p(t)) - 2 \frac{z_{p2*}(t)}{\tau_p} - \frac{v_{p2*}(t)}{\tau_p^2} \right) dt \quad (76)$$

$$dv_{p3*}(t) = z_{p3*}(t)dt \quad (77)$$

$$dz_{p3*}(t) = \left(\frac{\theta_{si}(t)}{\tau_{si}} c_4 g(v_{si}(t)) - 2 \frac{z_{p3*}(t)}{\tau_{si}} - \frac{v_{p3*}(t)}{\tau_{si}^2} \right) dt \quad (78)$$

$$dv_{p4*}(t) = z_{p4*}(t)dt \quad (79)$$

$$dz_{p4*}(t) = \left(\frac{\theta_{si}(t)}{\tau_{si}} c_6 g(v_{si}(t)) - 2 \frac{z_{p4*}(t)}{\tau_{si}} - \frac{v_{p4*}(t)}{\tau_{si}^2} \right) dt \quad (80)$$

$$dv_{p5*}(t) = z_{p5*}(t)dt \quad (81)$$

$$dz_{p5*}(t) = \left(\frac{\theta_{fi}(t)}{\tau_{fi}} c_7 g(v_{fi}(t)) - 2 \frac{z_{p5*}(t)}{\tau_{fi}} - \frac{v_{p5*}(t)}{\tau_{fi}^2} \right) dt \quad (82)$$

$$dv_{p6*}(t) = z_{p6*}(t)dt \quad (83)$$

$$dz_{p6*}(t) = \left(\frac{\theta_e(t)}{\tau_e} c_2 g(v_e(t)) - 2 \frac{z_{p6*}(t)}{\tau_e} - \frac{v_{p6*}(t)}{\tau_e^2} \right) dt \quad (84)$$

$$dv_{p7*}(t) = z_{p7*}(t)dt \quad (85)$$

$$dz_{p7*}(t) = \left(\frac{\theta_p(t)}{\tau_p} \mu - 2 \frac{z_{p7*}(t)}{\tau_e} - \frac{v_{p7*}(t)}{\tau_p^2} \right) dt + \frac{\theta_p(t)}{\tau_p} \epsilon(t) dW. \quad (86)$$

$$(87)$$

In these equations dW represents a Wiener process and is required as $\epsilon(t) \sim N(0, \sigma)$, where σ and μ (equation 21) describe the mean and variance of the stochastic model input. Further, $v_{po}(t)$ and $v_{p1-7*}(t)$ represent the membrane potential produced by each synapse and $z_{po*}(t)$ and $z_{p1-7*}(t)$ their derivatives. The inputs to each neural population are specified by $v_b(t)$ and $z_b(t)$, and are the membrane potential of the specific population, where b takes the values of p, e, fi and si representing pyramidal, excitatory, and slow and fast inhibitory populations, respectively. Therefore $v_p(t)$ is the output of the model. All $v_b(t)$ can be described in terms of $v_{po}(t)$ and $v_{p1-7}(t)$ as follows

$$v_p(t) = v_{p6*}(t) + v_{p7*}(t) - v_{p3*}(t) - v_{p5*}(t) \quad (88)$$

$$v_e(t) = v_{po*}(t) \quad (89)$$

$$v_{si}(t) = v_{p1*}(t) \quad (90)$$

$$v_{fi}(t) = v_{p2*}(t) - v_{p4*}(t). \quad (91)$$

Notice that equations 71-76 and equations 77-80 are identical except for the connectivity constants. Further, in this model it is assumed that

$$\theta_p = \theta_e \quad (92)$$

$$\tau_p = \tau_e. \quad (93)$$

Therefore, equations 83-86 are identical, but have different inputs. Next consider the effect of the states

$v_{p0-7*}(t)$ and $z_{p0-7*}(t)$ on the model inputs. Note that since the effect of $v_{p6*}(t)$ and $v_{p7*}(t)$ are additive, they can be added prior to being passed through the linear filter since

$$fx + fy = fx + y, \quad (94)$$

where f is defined above and x and y are arbitrary variables. Therefore equations 83-86 can be simplified to the following:

$$dv_{p1}(t) = z_{p1}(t)dt \quad (95)$$

$$dz_{p1}(t) = \left(\frac{\theta_e(t)}{\tau_e} (\mu + n_e g(v_e(t)) - 2\frac{z_{p1}(t)}{\tau_e} - \frac{v_{p1}(t)}{\tau_e^2}) \right) dt + \frac{\theta_e(t)}{\tau_e} \epsilon(t)dW. \quad (96)$$

. By making this reduction the effect of both the excitatory population and the input have been incorporated in one potential. Therefore, $v_{p7*}(t)$ is no longer required in equations 88.

Next consider the equations that only have connectivity constants that are different. Notice that these connectivity constants scale the input to the function, and this scaling can be performed after the input is transformed by the linear function. Therefore, equations 71-76 can be represented by a single equation such that

$$dv_{po}(t) = z_{po}(t)dt \quad (97)$$

$$dz_{po}(t) = \left(\frac{\theta_p(t)}{\tau_p} g(v_p(t)) - 2\frac{z_{po}(t)}{\tau_p} - \frac{v_{po}(t)}{\tau_p^2} \right) dt. \quad (98)$$

Notice that in doing this equations 89-91 are no longer valid and need to be altered to include the connectivities that have been removed from their relevant functions

$$v_e(t) = c_1 v_{po}(t) \quad (99)$$

$$v_{si}(t) = c_3 v_{p0}(t) \quad (100)$$

$$v_{fi}(t) = c_5 v_{p0}(t) - v_{p4*}(t). \quad (101)$$

A similar argument can be applied to equations 77-80 which can be simplified to

$$dv_{p2}(t) = z_{p2}(t)dt \quad (102)$$

$$dz_{p2}(t) = \left(\frac{\theta_{si}(t)}{\tau_{si}} g(v_{si}(t)) - 2\frac{z_{p2}(t)}{\tau_{si}} - \frac{v_{p2}(t)}{\tau_{si}^2} \right) dt. \quad (103)$$

Again by doing so equation 88 and 101 are no longer valid and become

$$v_p(t) = v_{p1}(t) - c_4 v_{p2}(t) - v_{p5*}(t) \quad (104)$$

$$v_{fi}(t) = c_5 v_{p0}(t) - c_6 v_{p2}(t). \quad (105)$$

. Lastly for simplicity equations 81-82 are replaced with

$$dv_{p3}(t) = z_{p3}(t)dt \quad (106)$$

$$dz_{p3}(t) = \left(\frac{\theta_{fi}(t)}{\tau_{fi}} c_7 g(v_{fi}(t)) - 2\frac{z_{p3}(t)}{\tau_{fi}} - \frac{v_{p3}(t)}{\tau_{fi}^2} \right) dt. \quad (107)$$

Which results in the set of equations demonstrated in the methods section. Notice that the n_b term used in the general form of the equations specifies connectivities that were not removed from the full model description equations due to simplification.

References

- Freeman, W. (1963). The electrical activity of a primary sensory cortex: analysis of eeg waves. *Int. Rev. Neurobiol*, 5:53–119.
- Jansen, B. and Rit, V. (1995). Electroencephalogram and visual evoked potential generation in a mathematical model of coupled cortical columns. *Biological Cybernetics*, 73(4):357–366.
- Lopes da Silva, F., Hoeks, A., Smits, H., and Zetterberg, L. (1974). Model of brain rhythmic activity. *Biological Cybernetics*, 15(1):27–37.
- Voss, H., Timmer, J., and Kurths, J. (2004). Nonlinear dynamical system identification from uncertain and indirect measurements. *International Journal of Bifurcation and Chaos*, 14(6):1905–1933.
- Wendling, F., Bartolomei, F., Bellanger, J., and Chauvel, P. (2002). Epileptic fast activity can be explained by a model of impaired GABAergic dendritic inhibition. *European Journal of Neuroscience*, 15(9):1499–1508.
- Wendling, F., Hernandez, A., Bellanger, J., Chauvel, P., and Bartolomei, F. (2005). Interictal to ictal transition in human temporal lobe epilepsy: Insights from a computational model of intracerebral EEG. *Journal of Clinical Neurophysiology*, 22(5):343.
- White, J., Banks, M., Pearce, R., and Kopell, N. (2000). Networks of interneurons with fast and slow γ -aminobutyric acid type a (gabaa) kinetics provide substrate for mixed gamma-theta rhythm. *Proceedings of the National Academy of Sciences*, 97(14):8128.
- Wilson, H. and Cowan, J. (1973). A mathematical theory of the functional dynamics of cortical and thalamic nervous tissue. *Biological Cybernetics*, 13(2):55–80.